2014 23rd International Lightning Detection Conference
18 - 19 March • Tucson, Arizona, USA
5th International Lightning Meteorology Conference
20 - 21 March • Tucson, Arizona, USA

Sensitive Measurement of Lightning Current and Charge Motion Using Coherent Averaging of Low Frequency Magnetic Field Observations

Joel L. Weinert, Steven A. Cummer
Department of Electrical and Computer Engineering
Duke University
Durham, NC, USA
joel.weinert@duke.edu

***Abstract*—Measuring lightning charge transfer, especially on time scales longer than several milliseconds, is a challenge. Instrumented towers can measure this quantity precisely but only for a tiny fraction of cloud-to-ground lightning. Electrostatic field measurements of lightning signals can provide robust estimates of this quantity, but the fast decay with distance of the electric field limits the measurement range to roughly 100 km at best. In contrast, low frequency and nearly-static magnetic fields from slowly varying lightning current decay much more slowly with distance and can therefore be measured at very long ranges. By measuring these low frequency magnetic fields, it is possible to broaden the geographic reach of lightning charge measurements. Sensitivity and noise, however, often limit these measurements to very large charge transfer lightning. Using data collected via search coil magnetic field sensors, we show how time-aligned coherent summation of many signals from lightning in a small geographic window can dramatically reduce the noise and thus enable the measurement of average (not individual) lightning currents and charge motion with very high precision and sensitivity. These average values (especially for long continuing currents) are often below the noise floor of remote measurement systems, especially for systems operating at long ranges (thousands of km) from the individual lightning events. Furthermore, by calculating averages over many thousands of lightning events, it is possible to achieve robust averages of different types of lightning under different storm conditions. Increasing the number of events analyzed further decreases the average noise received by the system, thus yielding improved results.**

Keywords—lightning discharge; lightning detection; lightning charge transfer; continuing current; coherent averaging

I. INTRODUCTION

A. Lightning Structure

Electrified clouds, such as those found in thunderstorms, can be modeled using a simple approximation of a positive charge on the order of tens of coulombs positioned above a negative charge mass of approximately equal magnitude (Fig. 1). Further simplifications model these separated charge masses as two oppositely charged point charges forming an electric dipole. Typical lightning events are classified based on the polarity and endpoints of the charge transferred – i.e. events that transfer negative charge from the cloud to ground are classified as negative cloud-to-ground events (–CG) while events that transfer net positive charge to ground are referred to as positive cloud-to-ground events (+CG). This work is primarily concerned with cloud-to-ground flashes, including both +CG and –CG events.

Many CG flashes contain multiple return strokes. After the conclusion of the initial return stroke, it is possible for future return strokes to propagate using the same conductive channel. These return strokes are delayed from previous strokes by anywhere from a few milliseconds to more than a hundred milliseconds [Berger et al., 1975]. –CG flashes with several dozen individual strokes have been observed and most –CG flashes consist of multiple return strokes. The majority of +CG flashes, however, consist of only a single return stroke [Beasley, 1985].

Furthermore, many CG flashes, especially +CG flashes, are followed by a continuing current on the order of a few hundred amps that can last hundreds of milliseconds. This continuing current does not occur in all CG flashes, but continuing current lasting more than 40 ms has been estimated to occur in less than 10% of negative flashes [Rakov and Uman, 1990a] and the majority of positive flashes [Rust et al., 1981]. Although the current magnitude of the continuing current is much lower than that of the return stroke, because of the greater time scale for continuing current compared to the return stroke, a significant portion of the total charge transfer of a flash may occur during the continuing current. Because of their role in the overall charge transfer of a lightning flash, the detection and measurement of continuing currents are of particular interest in characterizing the overall parameters of a particular flash or even a particular storm.

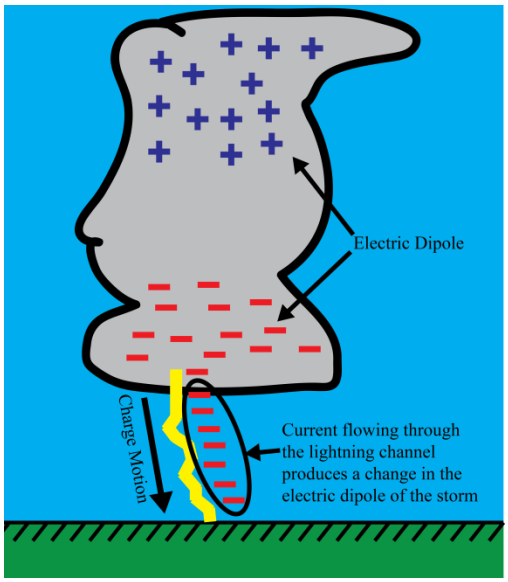

Fig. 1: Dipole structure of an electrified cloud

B. *Measuring Continuing Current*

Continuing current can be measured in three main ways, all of which have a well-established history in the field of lightning study. First, continuing current can be measured using instrumented towers which contain instruments capable of measuring currents flowing through the lightning channels (demonstrated by Fisher et al. [1993], among others). Although this method allows for very precise, accurate measurements, it is limited by the fact that the lightning flash of interest is required to actually strike the instrumented tower, meaning that very few lightning events are measured compared to the overall occurrence of lightning events in a particular storm.

Second, lightning can be calculated by measuring the change in the electric dipole structure of the storm. By measuring the change in the dipole structure of the electrified cloud, it is possible to calculate the amount and rate of charge being transferred during the return stroke and continuing current (such as in work done by Kitagawa et al. [1962], Rakov and Uman [1990b], and many others). The equation for electric field of a dipole is given in (1), where ε_0 is the free space permittivity, p is the magnitude of the separated charges, and r is the displacement between the dipole and the observer.

$$E = \frac{1}{4\pi\varepsilon_0}\frac{p}{r^3} \tag{1}$$

Because the field decreases at a rate of $1/\mathrm{r}^3$ with respect to the observer distance from the vertical charge dipole, this technique is limited to a range of about 100 km. As lightning flashes must occur relatively close to sensors capable of measuring the change in the electric dipole, a minority of flashes are measured using this technique.

Third, lightning currents can be calculated by measuring the magnetic field produced by the current flowing in the channel of the flash, which can be sensed using a simple small loop antenna. The magnetic field for a current-carrying wire can be described using (2), where μ_0 is the free space permeability, I is the current flowing the channel, and r is the distance from the channel to the observer.

$$B = \frac{\mu_0 I}{2\pi r} \tag{2}$$

This field decreases at a rate of $1/\mathrm{r}$ (as compared to $1/\mathrm{r}^3$ for the electric dipole field), meaning that it is possible to measure events at distances greater than 1000 km, as demonstrated by Cummer and Füllekrug [2001], among others. Measurements taken in this fashion are limited by system sensitivity and noise (both environmental noise and noise introduced by the sensor and data acquisition systems). Due to these limitations, direct observation and calculation of small signals, such as those of continuing current, are difficult to detect and measure over the noise floor of the measurement system.

II. Methodology

A. *Time Alignment*

Although individual events may not have a perceptible continuing current that is above the signal level of the noise floor, the small-magnitude continuing current still emits a signal which would be detectable given a sensor and environment with a low enough noise level. Because the majority of relevant noise sources (environmental and system) are generally broadband, by averaging signals together, the effective average noise level decreases by a factor of $1/\sqrt{\mathrm{n}}$, where n is the number of events being averaged.

For the sake of this work, a subset of events with similar characteristics was selected using National Lightning Detection Network (NLDN) data. A simple peak-search algorithm was used on low-frequency data to find the point of largest current moment magnitude (defined here to be $\mathrm{t} = 0$ for each event), assumed in this work to be the center of the return stroke. After detection, events were aligned with respect to the return stroke timing and averaged (Fig. 2). By performing this operation for many events, the noise can be observed to decrease by approximately the expected rate of $1/\sqrt{\mathrm{n}}$ (see Fig. 3 and Table 1). For this work, system noise is estimated by calculating the standard deviation of the signal over several seconds that are well-removed from the time-aligned return stroke.

B. *Waveform Extraction*

It is possible to calculate the effects of atmospheric propagation on a generated lightning signal using finite difference time domain (FDTD) methods. Specifically, Hu and Cummer [2006] used FDTD simulations to model the received response of an approximately impulse charge moment transfer for a variety of propagation distances. Convolving a different source current moment waveform with that of the impulse response for a given propagation distance yields the expected received signal at that distance for the given source current moment.

By comparing a variety of simulated waveforms to that of the averaged measurements, it is possible to extract an average source current moment for the selected events. It is significant to note that this source represents the average extracted source, but may not (and probably will not) be accurate for any individual events in the selected subset. However, this

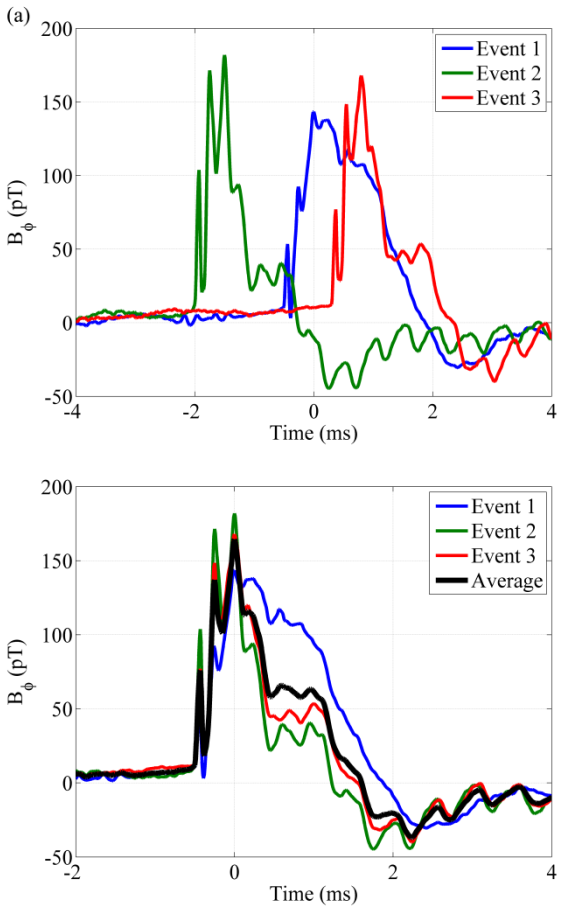

Fig. 2. (a) received lightning ULF waveforms (b) waveforms after time-alignment and averaging

extracted waveform is still useful, as it allows us to make generalizations on the whole about the subset of events that have been chosen for analysis, such as for a particular storm, or for a class of events in general.

C. Sensor Comparison

To verify the measured results of this work, multiple sensor systems with different frequency bandwidths were averaged and compared. These sensor systems have well-known (but different) frequency responses. Because the sensors were collocated geographically, the only difference between the recorded signals should be due to the measurement capabilities and frequency response characteristics of the systems. By appropriately digitally filtering the separate systems, it is possible to make a comparison between the two systems to validate the methodology used here.

The FDTD simulations (described above) naturally have a much greater bandwidth than those of the systems used in this work. By digitally filtering the simulated FDTD waveforms, it is possible to compare the FDTD simulation to the measured average for a given system. By altering the cutoff frequencies and other parameters of the filters applied to the FDTD results, the simulated signal can be compared to multiple sensor systems, therefore validating the results of the FDTD source waveform extraction.

TABLE I. COMPARISON OF MEASURED NOISE LEVELS

n	σ	Norm. σ	$1/\sqrt{n}$
1	31.412 pT	1.0000	1.0000
10	8.8187 pT	0.2807	0.3162
100	2.8367 pT	0.0903	0.1000
1000	711.09 fT	0.0226	0.0316

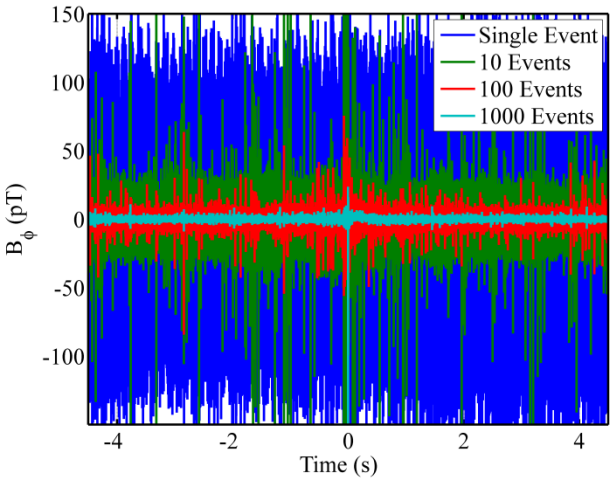

Fig. 3. Noise levels for increasing numbers of averaged events

Within this work, two sensor systems are considered, both located at the Duke Forest research station near Durham, N.C. (35.970° N, 79.094° W). The primary system utilized here is the EMI BF-4 (henceforth referred to as the BF-4 system), which covers the ULF frequency range. The second system utilized in this work is the magnetic field system manufactured by Quasar Federal Systems (referred to here as the QFS system), operating in the ELF/VLF range. For more information on the systems used here, see Table 2.

III. RESULTS

A. Event Selection

Event selection plays an important role in the process described in this paper. For this work, two categories of events were chosen for selection – +CG events and –CG events. Events were selected to have a range of approximately 1000 km – chosen because this distance was sufficiently great as to make most continuing currents undetectable using the chosen sensor systems, but still close enough that this methodology should reveal any average continuing current. Selected events were separated into subsets based on polarity.

Two further restrictions were placed on event selections. First, to ensure that the peak signal waveform magnitude is great enough to allow for automatic time-alignment, events selected were required to have a peak current magnitude of at least 20 kA. Signals lower than this threshold were predicted to be too likely to be considered noise and ignored. Also, as mentioned above, many CG flashes contain multiple return strokes. As continuing current may be present in the interstroke period, events were aligned using the first return stroke of the flash. For the sake of this work, return strokes are classified as

either first strokes or subsequent strokes, depending on their occurrence within the flash.

A single storm system was selected for analysis in this work. This storm was chosen because it occurred within the geographic distance of interest and also because it contained a high number of eligible lightning events. Furthermore, little lightning was occurring outside of the storm of interest, thus decreasing the chances of incorrect detection of a flash. The storm selected for analysis occurred between 1000 UTC on 24 September 2013 and 1000 UTC on 25 September 2013. This storm took place over the southern United States, primarily Mississippi, Alabama, and Florida (Fig. 4). A summary of the final event selections is given in Table 3. The ratio of events chosen is consistent with previously published values [Heidler and Hopf, 1998; Orville and Silver, 1997].

B. Positive CGs

Averaged results of +CGs are shown in Fig. 5. Typical lightning features, including the leader, return stroke, and continuing current, are visible. Because of the limited frequency bandwidth of the systems, as well as filtering, both hardware and digital, performed on the received signals, the systems both exhibit some overshoot (Fig. 5(a)). Although the waveforms may appear to be very different, many differences can be attributed to the different frequency responses of the systems. Several interesting features of the averaged waveforms merit specific mention.

First, the noise level of the signal is decreased to 209.2 fT, much lower than the single-event case of 31.42 pT. There is also a discernable continuing current, particularly in the BF-4

TABLE II. SYSTEM OPERATIONAL PARAMETERS

System	f_{low}	f_{high}	Hardware Filtering	f_s
BF-4	150 mHz	700 Hz	700 Hz LPF	2.5 kSa/s
QFS	2.1 Hz	25 kHz	25 kHz	100 kSa/s

Schumann Resonance signal is visible in both

TABLE III. EVENT SELECTION SUMMARY

Type	First Strokes	Subsequent Strokes	Avg. Peak Current (kA)
+CG	3,124	161	37.163
-CG	23,828	36,375	52.806

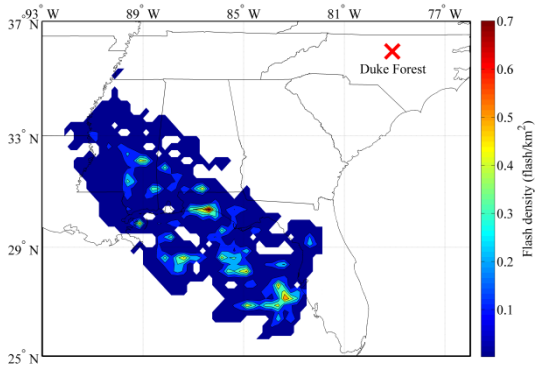

Fig. 4. Map of flash density for selected events

signal, of about 12 pT compared with the peak magnitude of 340 pT. The Schumann Resonance signal is visible in both sensor waveforms at about $t = 157$ ms (Fig. 5(c)). This signal is the original lightning signal travelling around the world in the opposite direction from the shortest distance path to the receiver and is typically buried within the noise of the receiver system. Next, there is clearly some charge motion happening well before the time-aligned return stroke. This charge motion is visible in the measured signal beginning at about $t = -1$ s. Because the magnitude of this signal is very small and is fairly low-frequency, it is nearly invisible in the QFS system and only obvious in the BF-4 system.

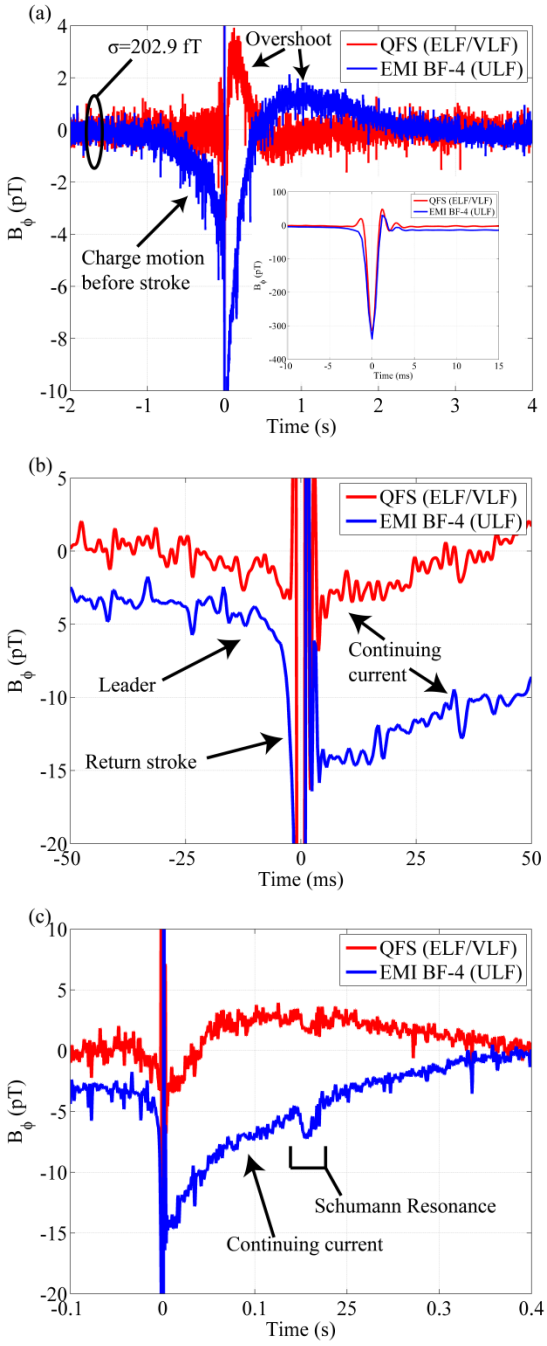

Fig. 5. Positive CG average waveforms on three different time scales

C. Negative CGs

The averaged waveforms for –CGs are given in Fig. 6. As with the +CG waveforms, the main components (leader, return stroke, continuing current) of the lightning flash are visible. However, several differences exist between the –CG and +CG waveforms. First, because of the greater number of events chosen, the noise level is lower in this case than when analyzing the +CG signals (82.12 fT for –CG, compared to 209.2 fT for +CG). The Schumann Resonance signals for –CG events are present at about the same time as those for the +CG events from the same storm. Of particular interest in this case is the fact that a second Schumann Resonance signal is visible at $t = 321$ ms. This second signal is the lightning signal circling the globe twice and is only visible because the greater number of –CG events allows for the average noise level to be decreased further.

One of the differences between the +CG and –CG cases investigated further is the difference in continuing current of the average waveforms. As mentioned previously, the +CG shows a continuing current signal of about 12 pT. Although the –CG events appear to also show some, albeit less, continuing current signal (about 2 pT), the influence of subsequent return strokes must be taken into account. Because the +CG events had a relatively low ratio of 0.052 subsequent to first strokes, any signal occurring after the time-aligned first stokes could be reasonably assumed to be due to continuing current. This assumption does not hold true for the –CG case, however, due to the higher ratio of large subsequent strokes to first strokes (1.527 for the selected storm).

To investigate this issue further, subsequent strokes were time-aligned and averaged. Because each subsequent stroke was preceded by at least one other return stroke, it is reasonable to assume to that any significant signal occurring before the $t = 0$ point of the subsequent strokes is at least partially influenced by the previous return strokes in the same flash. The results of this averaging are shown in Fig. 7. Some signal is clearly present before $t = 0$, which is attributable to both other return strokes and some interstroke continuing current. Because interstroke interval varies, it is difficult to extract how much of the signal following the return stroke is due to continuing current and how much is due to subsequent return strokes.

D. Extracted Source Currents

Using the methods described above, source current moment waveforms are extracted for both +CG and –CG events for the storm in question. The extracted source waveforms are convolved with an impulse response for a propagation distances corresponding to the range of the storm in question from the receiver. The high-bandwidth result of the convolution operation is then filtered appropriately for the two separate sensor systems in use at the receiver site.

After convolution, a comparison with the appropriate measured average waveforms is shown in Fig. 8 and Fig. 9. Correlation between the simulated, convolved waveforms and the measured average waveforms is high for both cases and both systems. The source current moment waveforms for the two cases are given in Fig. 10.

The source current moment waveform shows many features consistent with well-understood CG lightning processes, including a visible leader and return stroke. The waveform shows a clear leader motion beginning some tens of milliseconds before the return stroke (Fig. 10(a)) consistent with observed durations of stepped leaders [Rakov and Uman, 1990b].

Also present in the source waveform is some charge motion that continues after the conclusion of the return stroke (Fig. 10(b)). Using the method outlined in this work, some measurable charge motion (due to both continuing current and subsequent strokes) is present well after the conclusion of the

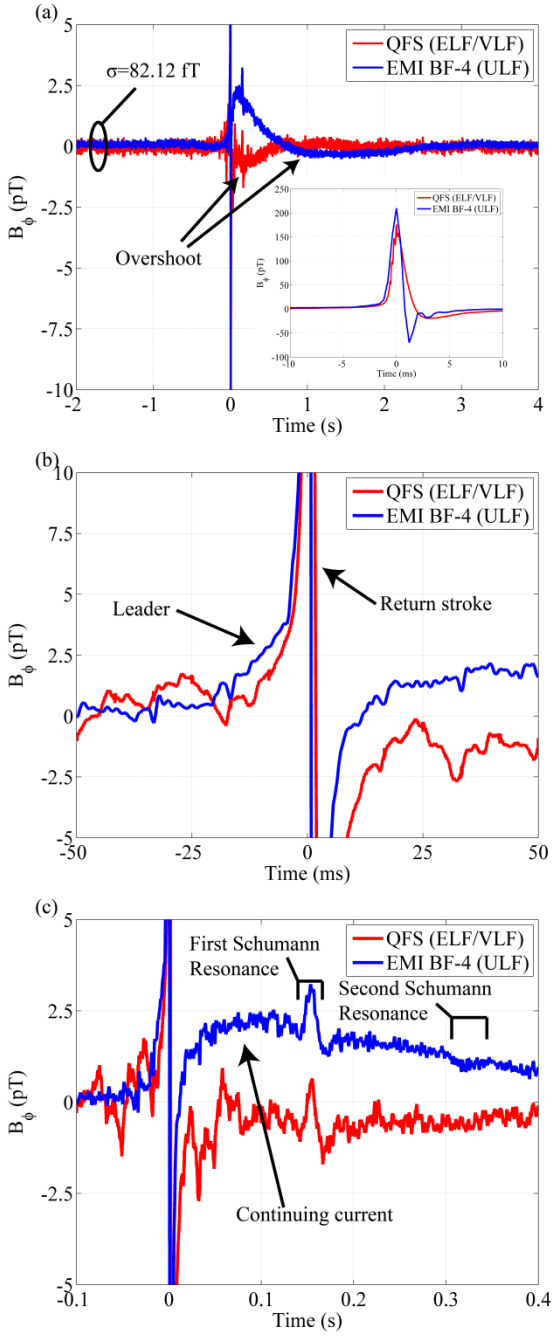

Fig. 6: Negative CG average waveforms on three different time scales

return stroke. Both continuing current and subsequent strokes, however, contribute to the total charge transferred to ground of the flash and are therefore valid contributions to the average flash waveform for the storm.

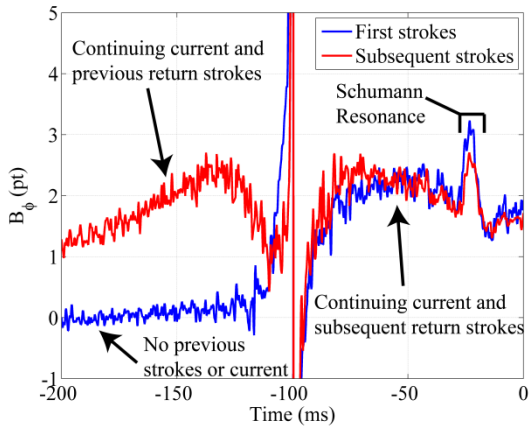

Fig. 7: Comparison of first and subsequent stroke averaging

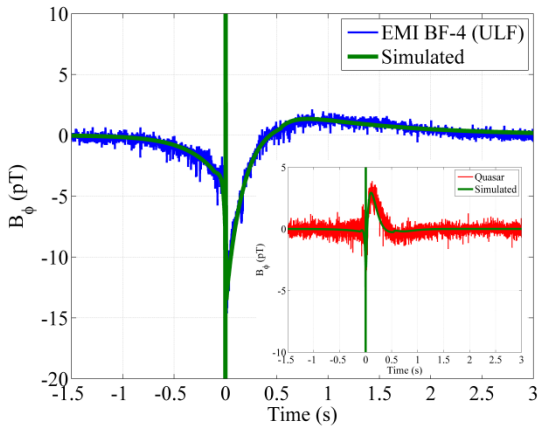

Fig. 8: Comparison between simulated and measured averages for BF-4 (main panel) and QFS (inset) systems for positive CGs

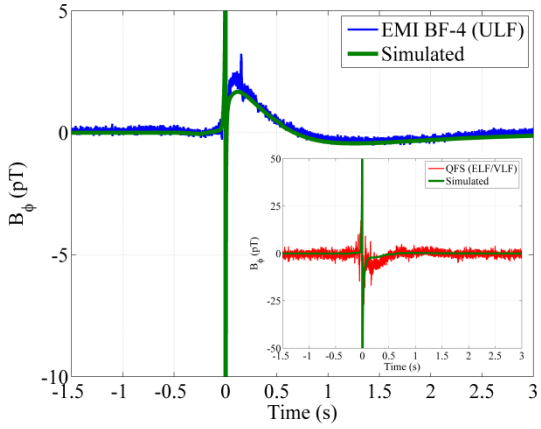

Fig. 9: Comparison between simulated and measured averages for BF-4 (main panel) and QFS (inset) systems for negative CGs

Charge motion is also visible before the return stroke in the both the +CG and –CG waveforms (Fig. 10(c)). For the +CG waveforms, this charge motion is clearly visible at $t = -1$ s, with a small polarity change at about $t = -100$ ms. This brief polarity change may be partially explained by pre-stroke intracloud charge transfer as described in Rust et al. [1981]. Some inverse pre-stroke motion is also visible in the –CG waveform. This process is not fully explained, but may be due in part to a minority of non-typical events such as "hybrid IC-NCG" flashes, as discussed by Lu et al. [2012].

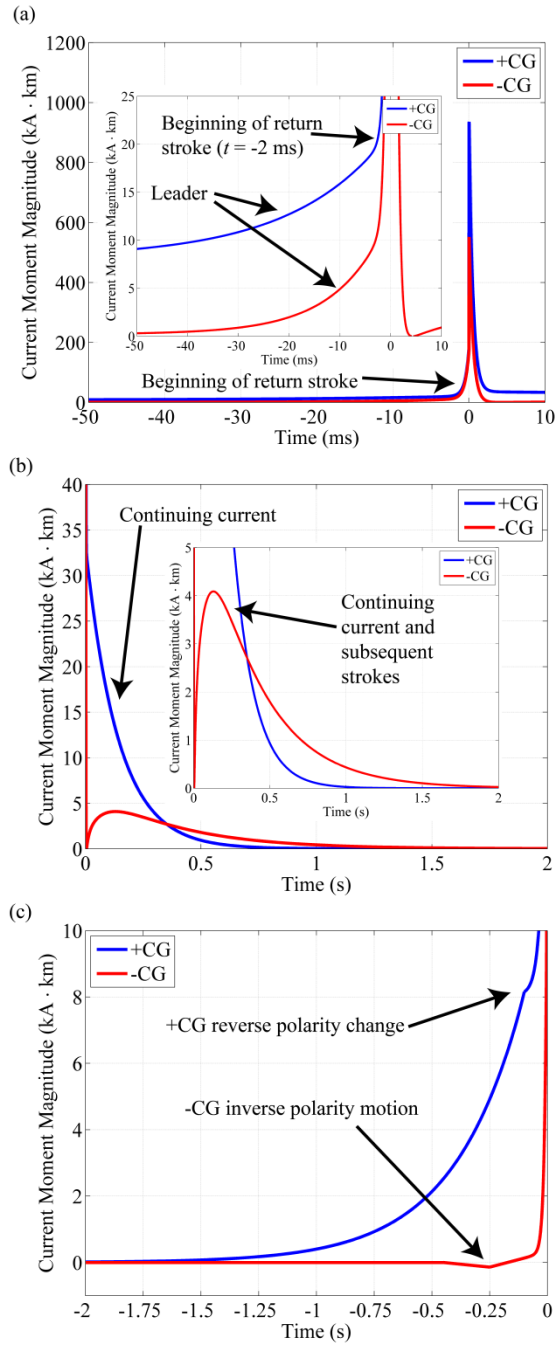

Fig. 10. Source current moment waveform (a) leader and return stroke (b) continuing current and subsequent strokes (c) prestroke charge motion

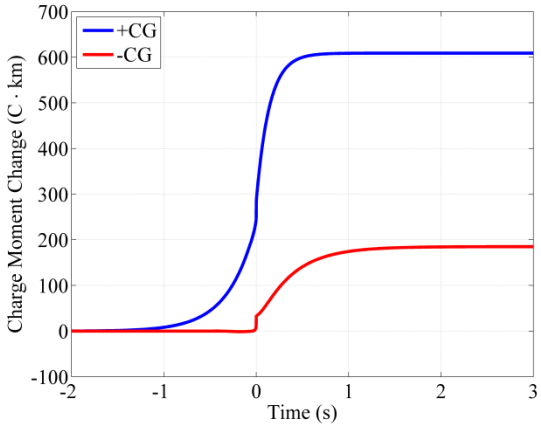

Fig. 11: Charge moment change of both positive CG and negative CG sources

By integrating the average source current waveforms, the average source charge moment for each polarity is obtained (Fig. 11). By assuming a typical channel length of 7 km, each average flash can be characterized by the amount and polarity of charge transferred to ground. If it is assumed that each of the selected flashes transfers this amount of charge to ground, a storm can be characterized by the amount of charge transferred to ground as a function of time, done in Fig. 12. This characterization is only an estimate however, as it assumes that all of the observed CG flashes transferred the average amount of charge, regardless of their individual characteristics.

IV. Conclusions

Of particular interest in the investigation of charge transferred during CG lightning flashes is that transferred during continuing current that occurs after the return stroke. Due to its long duration, charge transferred during the continuing current can represent a significant portion of the total charge transferred, but is difficult to measure by examining the change in the electric dipole field (range limitations) or using instrumented towers (small number of events). By examining magnetic fields associated with such continuing currents, measurements can be performed at very long ranges, including those greater than 1000 km. At such distances, noise and system sensitivity are often limiting factors.

This work has demonstrated a method of time-aligning and averaging many similar lightning events to obtain a single average waveform with drastically reduced noise. The noise of such an averaged signal decreases at the rate of $1/\sqrt{n}$. Using this method, waveforms for +CG and –CG events a selected storm were averaged and analyzed, demonstrating a noise level decrease from 31.42 pT to 82.12 fT. FDTD simulation allows for the extraction of source waveforms associated with each of the types of event. From these source waveforms, the charge and current moments are calculated, which can be used to calculate charge transferred per flash for an assumed channel length.

Although this work has focused on +CG and –CG events for a storm occurring 750-1250 km from the receiver, this method could be used to examine a variety of different lightning process which may fall below the noise floor of most

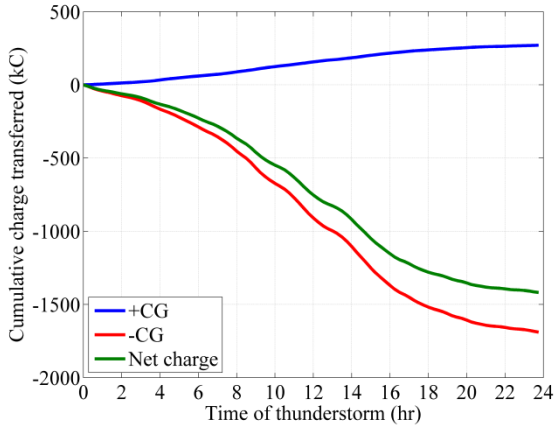

Fig. 12: Net charge transferred over life of thunderstorm

sensors. These interesting processes include, for example, narrow bipolar events (NBE) and terrestrial gamma-ray flashes (TGF), as well as oceanic storms, and storms at distances greater than those examined in this work.

References

Beasley, W. (1985), Positive cloud-to-ground lightning observations, *J. Geophys. Res.*, *90*(D4),6131–6138, doi:10.1029/JD090iD04p06131.

Berger, K., R.B. Anderson, and H. Kroninger (1975), Parameters of lightning flashes, *Electra*, *80*, 223-237.

Cummer, S., and M. Füllekrug (2001), Unusually intense continuing current in lightning produces delayed mesospheric breakdown, *Geophys. Res. Lett.*, *28*, 495-498, doi: 10.1029/2000GL012214.

Fisher, R. J., G. H. Schnetzer, R. Thottappillil, V. A. Rakov, M. A. Uman, and J. D. Goldberg (1993), Parameters of triggered-lightning flashes in Florida and Alabama, *J. Geophys. Res.*, *98*(D12), 22887–22902, doi:10.1029/93JD02293.

Heidler, F., and C. Hopf (1998), Measurement results of the electric fields in cloud-to-ground lightning in nearby Munich, Germany, *IEEE Trans. Electromagn. Compat.*, *40*(4), 436-443, doi: 10.1109/15.736204.

Hu, W. and S.A. Cummer (2006), An FDTD model for low and high altitude lightning-generated EM fields, *IEEE Trans. Antennas Propag.*, *54*, 1513-1522, doi: 10.1109/TAP.2006.874336.

Kitagawa, N., M. Brook, and E. J. Workman (1962), Continuing currents in cloud-to-ground lightning discharges, *J. Geophys. Res.*, *67*(2), 637–647, doi:10.1029/JZ067i002p00637.

Lu, G., S. A. Cummer, R. J. Blakeslee, S. Weiss, and W. H. Beasley (2012), Lightning morphology and impulse charge moment change of high peak current negative strokes, *J. Geophys. Res.*, *117*, D04212, doi:10.1029/2011JD016890.

Orville, R.E., and A.C. Silver (1997), Lightning ground flash density in the contiguous United States: 1992-1995, *Mon. Wea. Rev.*, *125*, 631-638.

Rakov, V. A., and M. A. Uman (1990a), Long continuing current in negative lightning ground flashes, *J. Geophys. Res.*, *95*(D5), 5455–5470, doi:10.1029/JD095iD05p05455.

Rakov, V. A., and M. A. Uman (1990b), Waveforms of first and subsequent leaders in negative lightning flashes, *J. Geophys. Res.*, *95*(D10), 16561–16577, doi:10.1029/JD095iD10p16561.

Rust, W. D., D. R. MacGorman, and R. T. Arnold (1981), Positive cloud-to-ground lightning flashes in severe storms, *Geophys. Res. Lett.*, *8*(7), 791–794, doi:10.1029/GL008i007p00791.